Sci Eng Compos Mater 19 (2012): 127–137 © 2012 by Walter de Gruyter • Berlin • Boston. DOI 10.1515/secm-2011-0103

The effect of multi-directional stiffness degradation on the non-linear analysis of composite laminates

Sung-Cheon Han[1], **Won-Hong Lee**[2]
and Weon-Tae Park[3,*]

[1] Department of Civil and Railroad Engineering, Daewon University College, 599 Shinwol, Jecheon, 390-702, Republic of Korea
[2] Department of Civil Engineering, Gyeongnam National University of Science and Technology, 150 Chilam, Jinju, 660-758, Republic of Korea
[3] Division of Construction and Environmental Engineering, Kongju National University, 275 Budai, Cheonan, 330-717, Republic of Korea, e-mail: pwtae@kongju.ac.kr

* Corresponding author

Abstract

A formulation of element-based Lagrangian 9-node shell element based modified first-order shear deformation theory is improved for non-linear behaviors of composite laminates containing matrix cracking. Using the refined ANS (assumed natural strain) shell elements either show the optimum combination of sampling points with an excellent accuracy or remove the locking phenomenon. The multi-directional stiffness degradation caused by matrix cracking, which was proposed by Duan and Yao, is conducted. Natural coordinate based higher-order transverse shear strains are used in the present shell element. Numerical examples demonstrate that the present element behaves reasonably satisfactorily either for the linear or geometrical non-linear analysis of laminated composite structures. The results of laminated composite shells with matrix cracking may be the benchmark test for the non-linear analysis of damaged composite laminates.

Keywords: assumed natural strain; element-based Lagrangian shell element; modified first-order shear deformation theory; non-linear analysis; stiffness degradation.

1. Introduction

The wide application of the fiber reinforced laminated composite shells in civil, marine, aerospace and other industries has found their advantages due to their high strength to weight ratio and their resistance to corrosion in comparison with the conventional metal shells. In recent years, the fatigue behavior of composite materials has been widely investigated. Basically, four main damage modes are inherent in laminated composite structures under fatigue loading: matrix cracking, delamination, fiber-matrix debonding and fiber breakage [1–3].

Various damage models have been developed to quantitatively evaluate the stiffness degradation of laminated composite structures due to transverse cracks in recent years, such as shear-lag model presented by Lim [4], damage model by Talerja [5], and experiential model by Fujii [6]. Generally, these models are developed only for the stiffness in the direction of loading. However, the fatigue damage is multi-directional and may cause stiffness reduction in some proportions under applied loading. Extensive understanding of the stiffness loss of laminated composite structures is necessary. The damage mechanics model to describe the stiffness properties under the cyclic loading was observed by Talerja [1, 5]. A new model by Duan and Yao [7] addresses the degradation of stiffness properties of laminated composite structures caused by matrix cracks. By using this model to describe the stiffness of composite laminate, only few constants need to be obtained from experiments.

To overcome the shear and membrane locking problems, Huang and Hinton [8] developed a 9-node assumed strain shell element using the enhanced interpolation of the transverse shear strains expressed in the natural coordinate system. The ANS (assumed natural strain) method can be traced to MacNeal [9] and Dvorkin and Bathe [10]. The ANS method and resultant shell element concept are used for composite shells in this study. The element-based Lagrangian formulation by Kanok-Nukulchai and Wong [11] will be used as it makes implementation simpler and easier than the traditional Lagrangian formulations, especially when the ANS method is involved.

The first-order shear deformable shell elements are capable of producing good results for the in-plane strain and stress distributions; however, their formulation results in constant transverse shear strains as opposed to the realistic parabolic distribution. They also require shear correction coefficients to recover the corresponding strain energy. Numerous efforts have been made to overcome the disadvantage of the first-order formulation. Tanov and Tabiei [12] presented an approach for treating the transverse shear strains and stresses in homogeneous shells resulting in parabolic distribution for both strains and stresses. Thus, it eliminates the need of any shear correction factors. It requires only minor changes in the first-order shear deformation formulation.

In this study, the 9-node ANS shell element is used in the non-linear analysis of composite plates and shells subjected to multi-directional stiffness degradation. To eliminate both the shear locking and the membrane locking, the assumed strain method by Han et al. [13] was applied in the framework of element natural coordinates. With arbitrary size of matrix cracking, the geometrical non-linear analyses of plate and shell structures are conducted. To validate the present shell element models, numerical examples are investigated in comparison with those solutions from the literature.

2. Stiffness degradation induced by matrix cracking

To simplify the problem, it is assumed that the matrix cracks are uniformly distributed in the off-axis plies [7] under uniaxial tensile loading. Thus, the main damage mode in the laminate is matrix cracking in the off-axial plies.

Consider a matrix cell, which contains matrix crack as shown in Figure 1, the relationship between the strain and the stress can be obtained as follows:

$$\begin{Bmatrix}\varepsilon_{11}\\ \varepsilon_{22}\\ 2\varepsilon_{44}\\ 2\varepsilon_{55}\\ 2\varepsilon_{66}\end{Bmatrix}=\begin{bmatrix}S_{11} & S_{12} & 0 & 0 & 0\\ & S_{22} & 0 & 0 & 0\\ & & S_{44} & 0 & 0\\ & symm. & & S_{55} & 0\\ & & & & S_{66}\end{bmatrix}\begin{Bmatrix}\sigma_{11}\\ \sigma_{22}\\ \sigma_{44}\\ \sigma_{55}\\ \sigma_{66}\end{Bmatrix}$$

$$=\begin{bmatrix}\frac{1}{E^m} & -\frac{\nu_{12}^m}{E^m} & 0 & 0 & 0\\ -\frac{\nu_{12}^m}{E^m} & \frac{1}{E^m}+\frac{4\pi \mathrm{T}^2}{E^m} & 0 & 0 & 0\\ 0 & 0 & \frac{1}{G_{23}^m} & 0 & 0\\ 0 & 0 & 0 & \frac{1}{G_{13}^m} & 0\\ 0 & 0 & 0 & 0 & \frac{1}{G_{12}^m}+\frac{4\pi \mathrm{T}^2}{E^m}\end{bmatrix}\begin{Bmatrix}\sigma_{11}\\ \sigma_{22}\\ \sigma_{44}\\ \sigma_{55}\\ \sigma_{66}\end{Bmatrix} \quad (1)$$

where E^m, G^m_{12} and ν^m_{12} are the elastic modulus, the shear modulus and Poisson's ratio of the undamaged matrix, and T was defined as the damage variable as

$$\mathrm{T}=\frac{c}{\sqrt{ab}}=\frac{c}{\sqrt{S_e}} \quad (2)$$

in which S_e is the area of the basic cell. By this definition, T can be regarded as the ratio of characteristic crack length to characteristic cell size, and its value can be obtained from experiments.

The modulus and Poisson's ratio of the damaged matrix are given as:

$$E_1^{mc}=E^m, \quad (3a)$$

$$E_2^{mc}=\frac{E^m}{1+4\pi \mathrm{T}^2}, \quad (3b)$$

$$G_{12}^{mc}=\frac{E^m}{2\left(1+\nu_{12}^{mc}\right)+4\pi \mathrm{T}^2}, \quad (3c)$$

$$G_{23}^{mc}=G_{23}^m=\frac{E^m}{2(1+\nu_{23}^{mc})}, \quad (3d)$$

$$G_{13}^{mc}=G_{13}^m, \quad (3e)$$

$$\nu_{12}^{mc}=\nu_{23}^{mc}=\nu_{13}^{mc}=\nu_{12}^m. \quad (3f)$$

Suppose there is a single ply containing parallel and uniformly distributed matrix cracks as shown in Figure 1. As only the matrix crack is considered, the composite ply can be regarded as the mixture of damaged matrix and undamaged fibers. Its stiffness property can be described according to the meso-model. Based on the widely accepted Tsai-Halpin model [14], the stiffness degradation of a single ply can be obtained as follows:

$$E_1=E^fV^f+E_1^{mc}(1\text{-}V^f), \quad (4a)$$

and

$$\nu_{12}=\nu^fV^f+\nu_{12}^{mc}(1\text{-}V^f). \quad (4b)$$

where E^f is the elastic modulus of the fiber, E_l^{mc} is the longitudinal tensile modulus of the damaged matrix, ν^f and ν_{l2}^{mc} are Poisson's ratios of the fiber material and damaged matrix material, respectively, and V^f is the fiber volume fraction of the ply. Thus,

$$\frac{M}{M^{mc}}=\frac{1+\xi\eta V_f}{1\text{-}\eta V_f} \quad (5)$$

where

$$\eta=\frac{\left(M^f/M^{mc}\right)\text{-}1}{\left(M^f/M^{mc}\right)+\xi} \quad (6)$$

in which M=composite modulus E_2, E_3, E_{12}, G_{12}, G_{23}, G_{13}, ν_{23}, ν_{13}, M^f=corresponding fiber modulus E^f, G^f, ν^f, M^{mc}=corresponding damaged matrix modulus E^{mc}, G^{mc}, ν^{mc} and ξ is a constant parameter of the material with a value that varies between 0 and ∞.

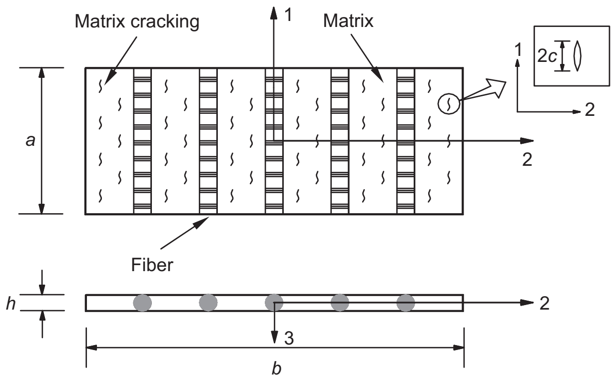

Figure 1 Composite plate which contains matrix crack.

3. Finite element method

3.1. Geometry and natural strains of the shell element

The higher-order shear deformation theory to be developed is based on the same assumptions as the first-order shear deformation theory, except that we relax the assumption on the straightness and normality of a transverse normal after deformation by expanding the displacements as cubic functions of the thickness coordinate. We start with the third-order displacement field.

$$\mathbf{P}(\xi_i)=\bar{\mathbf{P}}(\xi_\beta)+\xi_3\,\bar{\mathbf{V}}(\xi_\beta)+\xi_3^2\boldsymbol{\Phi}(\xi_\beta)+\xi_3^3\boldsymbol{\Psi}(\xi_\beta)\ ;\ i=1,2,3,\ \beta=1,2 \tag{7}$$

$$\mathbf{u}(\xi_i)=\bar{\mathbf{u}}(\xi_\beta)+\xi_3\,\bar{\mathbf{e}}(\xi_\beta)+\xi_3^2\boldsymbol{\varphi}(\xi_\beta)+\xi_3^3\boldsymbol{\psi}(\xi_\beta) \tag{8}$$

where $\mathbf{P}$ denotes the position vector of a generic point in the shell element; $\bar{\mathbf{P}}$ and $\bar{\mathbf{V}}$ are the position vector of a point in the mid-surface and a normal vector to the mid-surface; $\bar{\mathbf{u}}$ and $\bar{\mathbf{e}}$ are the translational displacement vector and the fiber displacement vector, respectively, of a point in the mid-surface; $\boldsymbol{\Phi}$, $\boldsymbol{\Psi}$ and $\boldsymbol{\varphi}$, $\boldsymbol{\psi}$ are the higher-order terms in $\mathbf{P}(\xi_i)$ and $\mathbf{u}(\xi_i)$, respectively.

Vanishing of the transverse natural shear stress at the top and bottom shell surfaces, $\tilde{S}_{23}(\pm1)=\tilde{S}_{13}(\pm1)=0$, makes the corresponding natural strains there zero. Using these relationships and the tensor transformation of Green strains, the transverse natural shear strains can be obtained (Tanov and Tabiei [12]).

$$\tilde{E}^s_{\alpha3}=\frac{1}{2}\left[\frac{\partial\bar{\mathbf{P}}_I}{\partial\xi_\alpha}\bar{\mathbf{e}}_I+\frac{\partial\bar{\mathbf{u}}_J}{\partial\xi_\alpha}\bar{\mathbf{V}}_J\right]\left(1-\xi_3^2\right)=\tilde{E}^{s1}_{\alpha3}+\tilde{E}^{s2}_{\alpha3} \tag{9}$$

We assumed that the lower-order terms in the expressions for in-plane shear strains based on the higher-order shear deformation theory by Reddy [15] represent their through-thickness distribution with sufficient accuracy. These expressions are identical to the strain expression from the first-order shear deformation theory, except for the transverse natural shear strain expressions, which include the higher-order terms that result in their parabolic through-thickness distribution.

The incremental form of the displacement field may be written in terms of the nodal incremental vector $\Delta\mathbf{u}^a$ as:

$$\Delta\mathbf{u}(\xi_1,\xi_2,\xi_3)=\sum_{a=1}^{9}N^a(\xi_1,\xi_2)\left[\mathbf{I}_{3\times3}\quad \xi_3\frac{h^a}{2}\mathbf{H}^a\right]\Delta\mathbf{u}^a \tag{10}$$

where $\Delta\mathbf{u}^a=\left\{\Delta\bar{u}_1^a,\Delta\bar{u}_2^a,\Delta\bar{u}_3^a,\Delta\theta_1^a,\Delta\theta_2^a,\Delta\theta_3^a\right\}$ and $\mathbf{H}^a$ is the rotational matrix of the normal vector at node a [13].

The incremental membrane, bending and transverse shear strains can be separated into the linear and the non-linear parts. The linear strain part can be expressed as:

$$\Delta\tilde{E}^m=\tilde{\mathbf{B}}_m\,\Delta\bar{\mathbf{u}},\ \Delta\tilde{E}^b=\xi_3\tilde{\mathbf{B}}_b\,\Delta\mathbf{u},\ \Delta\tilde{E}^s=\tilde{\mathbf{B}}_s\,\Delta\mathbf{u}. \tag{11}$$

Based on the assumed strains $\tilde{\mathbf{e}}$ in the present shell element, the relationship between the assumed strain and the nodal displacement matrix, i.e., $\tilde{\mathbf{B}}_{AS}$ can be further implemented instead of the standard $\tilde{\mathbf{B}}$ matrix, as shown in Eq. (12).

$$\begin{Bmatrix}\Delta^L\tilde{E}^m\\ \Delta^L\tilde{E}^b\\ \Delta^L\tilde{E}^s\end{Bmatrix}=\begin{bmatrix}\left(\tilde{\mathbf{B}}_{\mathbf{m}}\right)_{\mathrm{AS}} & 0\\ \xi_3\tilde{\mathbf{B}}_{b1} & \xi_3\tilde{\mathbf{B}}_{b2}\\ \left(\tilde{\mathbf{B}}_{\mathbf{s1}}\right)_{\mathrm{AS}} & \left(\tilde{\mathbf{B}}_{\mathbf{s2}}\right)_{\mathrm{AS}}\end{bmatrix}\begin{Bmatrix}\Delta\bar{\mathbf{u}}\\ \Delta\theta\end{Bmatrix} \tag{12}$$

where $\tilde{E}^m$, $\tilde{E}^b$ and $\tilde{E}^s$ are membrane, bending and transverse shear strain components derived by Han et al. [13].

3.2. The torsional effect

In this study, based on the procedure proposed by Kanok-Nukulchai [16], the drilling degree of freedom will be tied to the in-plane twist by a penalty functional through additional strain energy as:

$$U_t=k_tG\int_{V^e}\left[\alpha_t(\xi_1,\xi_2)-\frac{1}{2}\left\{\frac{\partial w_2}{\partial z_1}(\xi_1,\xi_2,0)-\frac{\partial w_1}{\partial z_2}(\xi_1,\xi_2,0)\right\}\right]^2dV \tag{13}$$

where w_1 and w_2 are displacement components in the local coordinate system; α_{t} is the in-plane torsional rotation; k_{t} is a parameter to be determined (the value of 0.1 suggested by Kanok-Nukulchai, [16]); G is the shear modulus; and V^e is the volume of the element. A two-by-two Gauss integration scheme is applied to evaluate the torsional stiffness to avoid the over-constrained situation. After integration throughout the thickness, Eq. (13) can be written as:

$$U_t=2k_tG\int_{-1}^{1}\int_{-1}^{1}\left[\alpha_t(\xi_1,\xi_2)-\frac{1}{2}\left\{\frac{\partial w_2}{\partial z_1}(\xi_1,\xi_2,0)-\frac{\partial w_1}{\partial z_2}(\xi_1,\xi_2,0)\right\}\right]^2 d\xi_1\,d\xi_2 \tag{14}$$

To derive a torsional stiffness from Eq. (14), the local variables are expressed in terms of global nodal variables by shape functions using virtual work principle. Thus, Eq. (14) can be expressed in the form:

$$\delta U_{\mathrm{t}}=\delta\mathbf{u}^T\mathbf{K}_{tL}\mathbf{u} \tag{15}$$

As the virtual displacement $\delta\mathbf{u}$ is arbitrary, the torsional stiffness matrix ($\mathbf{K}_{tL}$) can be obtained. This torsional stiffness term can be added as described in Kanok-Nukulchai [16].

4. Strain energy and stress resultants of composite laminates

The strain energy U of the shell-like three-dimensional body is given by the expression, where in curvilinear coordinates the stress tensor S_{ij} is contracted with the strain tensor E_{ij}, as:

$$U=\frac{1}{2}\int_V S_{ij}E_{ij}\,dV \tag{16}$$

In the laminated structures, the stiffness properties are functions of the normal coordinate. In Figure 2, a cross-section

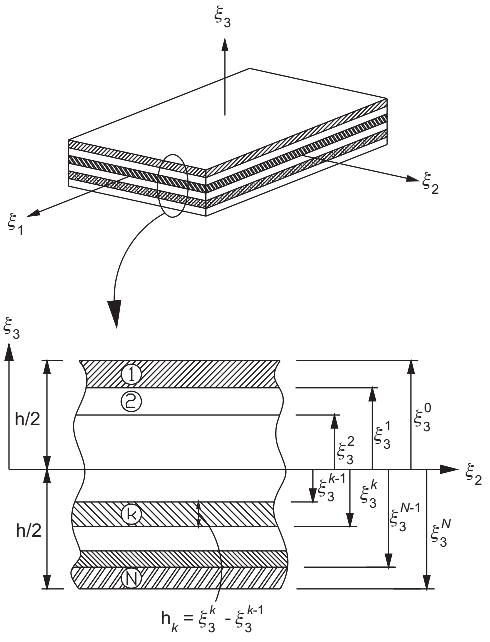

Figure 2 Cross-section of composite laminates composed of *N* layers.

of laminated plate composed of *N* layers is presented. Linear elastic properties of the anisotropic layers are characterized by the elasticity tensor C_{ijkl}. In this case, the Hook's law for each layer can be written by:

$$S_{ij}=C_{ijkl}E_{kl} \tag{17}$$

As the present formulation is based on the natural coordinate reference frame, here we introduce an explicit transformation scheme between the natural coordinate and the global coordinate systems, to obtain a natural coordinate based constitutive equation [13, 17]. The stress tensor in the natural coordinate system can be written as follows:

$$\tilde{S}_{ij}=\tilde{C}_{ijkl}\tilde{E}_{kl}=\tilde{J}_0\mathbf{T}\tilde{D}_{ijkl}\mathbf{T}^T\tilde{E}_{kl} \tag{18}$$

where $\tilde{J}_0$ is the determinant of the Jacobian matrix and $\tilde{D}_{ijkl}$ is the constitutive matrix for orthotropic materials with the material angle θ. The transformation matrix **T** in Eq. (18) is given by Han et al. [17]. Substituting Eq. (18) into Eq. (16) yields the strain energy *U* as:

$$U=\frac{1}{2}\int_A\int_{-h/2}^{h/2}\tilde{E}_{ij}^T\tilde{C}_{ijkl}\tilde{E}_{kl}\,d\xi_3\,dA \tag{19}$$

The plane stress condition $\tilde{S}_{33}=0$ and symmetry of both $\tilde{S}_{ij}$ and $\tilde{E}_{kl}$ are enforced. After integration, through the thickness, the strain energy can be obtained in terms of the laminated shell stiffness characteristics, i.e.:

$$A_{\alpha\beta},B_{\alpha\beta},D_{\alpha\beta}=\int_{-h/2}^{h/2}\tilde{C}_{\alpha\beta}(1,\xi_3,\xi_3^2)d\xi_3 \quad (\alpha,\beta=1,2,6) \tag{20a}$$

$$A_{\gamma\delta},D_{\gamma\delta},F_{\gamma\delta}=\int_{-h/2}^{h/2}\tilde{C}_{\gamma\delta}\left(1,\xi_3^2,\xi_3^4\right)d\xi_3 \quad (\gamma,\delta=4,5) \tag{20b}$$

where $A_{\alpha\beta}$, $B_{\alpha\beta}$ and $D_{\alpha\beta}$ are membrane, membrane-bending coupling and bending stiffness coefficients, respectively; $A_{\gamma\delta}$, $D_{\gamma\delta}$ and $F_{\gamma\delta}$ are shear stiffness coefficients, respectively. Note that the shear stiffness $D_{\gamma\delta}$ and $F_{\gamma\delta}$ of the third-order theory involve higher powers of the thickness. The matrices in Eq. (20a) are of the order 3×3 and those in Eq. (20b) are of order 2×2.

In the present study, a "modified" first-order shear deformable theory is proposed. It eliminates the need for shear correction factors in the first-order theory.

In the present shell element, resultant forces acting on a laminate are obtained by integration of stresses through the individual laminate thickness. We also impose the plane-stress state on the natural constitutive equation of Eq. (18) before forming the equivalent constitutive equation. Finally, the constitutive relations of the composite laminate are as follows:

$$\begin{Bmatrix} N_\alpha \\ M_\alpha \end{Bmatrix}=\begin{bmatrix} A_{\alpha\beta} & B_{\alpha\beta} \\ B_{\alpha\beta} & D_{\alpha\beta} \end{bmatrix}\begin{Bmatrix} \tilde{E}_\beta^m \\ \tilde{E}_\beta^b \end{Bmatrix} \tag{21a}$$

$$\begin{Bmatrix} Q_\gamma \\ R_\gamma \end{Bmatrix}=\begin{bmatrix} A_{\gamma\delta} & D_{\gamma\delta} \\ D_{\gamma\delta} & F_{\gamma\delta} \end{bmatrix}\begin{Bmatrix} \tilde{E}_\delta^{s1} \\ \tilde{E}_\delta^{s2} \end{Bmatrix} \tag{21b}$$

5. Incremental equation of equilibrium

The generalized Hook's law at large strain does not represent an approximate material behavior description because stress-strain relation is non-linear. From a practical point of view, Hook's law is only applicable to small strain, which constitutive tensor is constant coefficient. Using small strain assumption, the following incremental equilibrium equation is obtained.

$$\int\delta\left(\Delta^L\tilde{E}\right)^T\tilde{\mathbf{C}}\Delta^L\tilde{E}\,dV+\int\mathbf{S}\delta\left(\Delta^{NL}\tilde{E}\right)dV={}^{t+\Delta t}\delta W_{ext} -\int\delta\left(\Delta^L\tilde{E}\right)^T\mathbf{S}\,dV \tag{22}$$

where superscript *t* which is generally used as the current configuration is ignored in Eq. (22) and superscript $t+\Delta t$ is the adjust incremented configuration, ${}^{t+\Delta t}\delta W_{ext}$ is the external virtual work in $t+\Delta t$.

The total tangent stiffness comprises the material stiffness and the geometric stiffness. The linear part of the Green strain tensor is used to derive the material stiffness matrix and non-linear part of the Green strain tensor is used to derive the geometric stiffness matrix.

5.1. Linear element stiffness matrix

If the strain-displacement Eq. (12) is substituted into Eq. (22), the linear element material stiffness matrix ($[\mathbf{K}_L]$) is obtained.

$$\int\delta(\Delta^L\tilde{E})^T\tilde{\mathbf{C}}\,\Delta^L\tilde{E}\,dV=\delta\Delta\mathbf{u}^\mathbf{T}\left(\int\tilde{\mathbf{B}}^\mathbf{T}\tilde{\mathbf{C}}\tilde{\mathbf{B}}\,dV\right) \Delta\mathbf{u}=\delta\Delta\mathbf{u}^\mathbf{T}\left[\mathbf{K}_L\right]\Delta\mathbf{u} \tag{23}$$

For laminated composite structures, the stress resultant form which is called the equivalent constitutive equations as derived in Eq. (21) are used to capture layer effect through the thickness direction. The element stiffness matrix may be written in a matrix form using the equivalent constitutive equations. Finally, the element stiffness matrix has 6×6 sizes on the reference-surface of shell element. The torsional stiffness term is formed as described in Kanok-Nukulchai [16] and added to the stiffness term.

5.2. Geometric stiffness matrix

To obtain an accurate geometric stiffness matrix, the stresses should be evaluated accurately. The accuracy of the computation of stresses for formulation of geometric stiffness matrix is maintained by obtaining the same interpolated strains in the computation of linear stiffness matrix. The stresses are computed at the integration points based on these strains. Substituting the non-linear part of strain into Eq. (22), the following geometric stiffness matrix($[\mathbf{K}_G]$) is obtained [13].

$$\int \mathbf{S}\delta\left(\Delta^{NL}\tilde{E}\right)dV=\delta\Delta\mathbf{u}^{\mathrm{T}}\left(\int \tilde{\mathbf{G}}^{\mathrm{T}}\mathbf{S}\tilde{\mathbf{G}}\,dV\right)\Delta\mathbf{u}=\delta\Delta\mathbf{u}^{\mathrm{T}}\left[\mathbf{K}_G\right]\Delta\mathbf{u} \quad (24)$$

The geometric stiffness matrix in the natural coordinate is analytically integrated through the thickness. By the transformation the natural to the global frame, the element geometric stiffness matrix is obtained on the global frame with 6×6 submatrix.

Then, the final assembled incremental non-linear equilibrium equation can be written as:

$$\left([\mathbf{K}_L]+[\mathbf{K}_G]\right)\Delta\mathbf{u}={}^{t+\Delta t}\bar{\mathbf{F}}\text{-}\mathbf{F} \quad (25)$$

where $\bar{\mathbf{F}}$ and $\mathbf{F}$ are the external and internal forces, respectively.

The equilibrium equation must be satisfied throughout the complete history of loading and the non-linear processing will be stopped only when the out-of-balance forces are negligible within a certain convergence limit. If it is necessary to extend the stability analysis beyond the limit point, i.e., in the so-called post-buckling range, appropriate solution procedures must be applied. One approach is to use the arc-length control method in conjunction with the Newton-Raphson method to extend the stability analysis beyond the limit point, by Crisfield [18].

6. Numerical examples

Several numerical examples are solved to test the performance of the shell element in both linear and geometrically non-linear applications. Examples include isotropic materials to check crucial features and anisotropic composite materials for the comparisons and further developments. Before general various sections, linear and non-linear examples are treated. First, linear laminated composite plates are presented for comparison with Navier's solutions. Second, non-linear isotropic L-shape plate strip is presented for geometrically non-linear comparison. And finally, more general shell examples are treated with various fiber angles for parameter studies. The present element-based Lagrangian formulation is implemented in the FEAP program (Zienkiewicz and Taylor [19]).

6.1. Laminated composite plate

To validate the present shell element, several numerical examples of plates and shells are solved. The data for single ply and the initial elastic modulus of the laminates are listed in Table 1.

Table 2 shows the experimental results and prediction of the initial modulus of the lamina.

Examples are anisotropic undamaged and damaged composite materials for the comparisons and further developments. Quarter plate (Figure 3) under uniform loading is analyzed with 4×4 mesh sizes. The boundary condition is simply supported (a=b, a/h=100) and material properties are shown in Table 2. The mth layer (m=1,2,…, N) is oriented at an arbitrary angle θ_{m}, with respect to the plate coordinate axes.

The fiber volume fraction of the ply is V^f=0.45. From the initial stiffness of undamaged single ply, the constant ξ can be obtained as 4.12 with Eqs. (3b), (5) and (6). Before proceeding with the following study, the comparison with Navier's solution is presented. Results of the comparison study are shown in Table 3.

The results using a regular mesh show an excellent correlation to the results given by analytical solutions.

6.2. L-shape plate strip

A flat L-shaped plate strip is fully clamped along one edge and subjected to an in-plane point load at the free end (Figure 4). The material properties are E=71,240 N/mm^2 and ν=0.31. The plate is tilted initially with a slope of 1:250,000 to initiate non-neutral stability solution after the bifurcation point (buckling). Meshes consisting of 13×1 9-node elements are adopted to evaluate the convergence of the present shell element. In Figure 5, comparison is obtained between the results from the present formulation using as few as 13 elements, the results of the 6-node triangular shell formulation [20] with 68×2 elements, and the results of the 4-node

Table 1 Mechanical properties of fiber and matrix of the lamina.

	E (GPa)	G_{12} (GPa)	ν_{12}
Fiber	84.0	33.6	0.27
Matrix	3.2	1.26	0.27

Table 2 The comparison of the initial modulus between reference and this study.

	E_1 (GPa)	E_2 (GPa)	G_{12} (GPa)	ν_{12}
Duan and Yao [7]				
Experiment	41.7	13.0	3.4	0.3
Prediction	39.6	12.9	5.13	0.26
Present	39.56	12.99	5.13	0.27

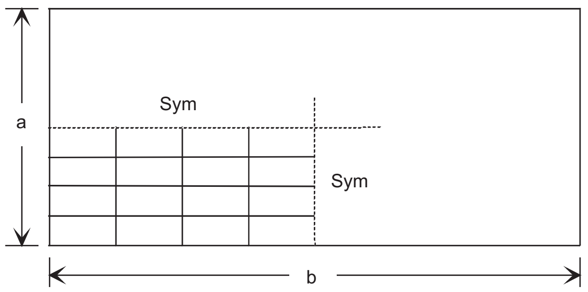

Figure 3 Simply supported and clamped rectangular plate.

enhanced assumed strain (EAS) formulation [21] using 68 elements, thus highlighting the effectiveness on the proposed present formulation.

In all cases of damaged composite plates and shells, the material properties of Table 2, the fiber volume fraction V^f=0.45 and the constant ξ=4.12 are used in computing the numerical values. The total thickness of the laminated is h=0.6 mm and all layers have the same thickness. Figure 6 shows the tip deflections of L-shape composite plates under the increased in-plane loads after initial buckling. The undamaged and damaged composites are used. For a plate with four numbers of alternate layers (45°/-45°/45°/-45°), the post-buckling paths show similar trends regardless of the crack ratio. As the parameter T (crack ratio) increases, the critical loads of the plate decrease. It is predictable because it is expected that an increased crack ratio results in worse rigidity for increased buckling load.

It may be noted that the load-deflection curve of undamaged L-shape composite plate with the fiber angle of (45°/-45°/45°/-45°) exhibits the higher value than damaged plates by 20–30%.

Figure 7 shows the tip deflection of the free end of anti-symmetric laminated composite plates (θ/-θ/θ/-θ) subjected to the in-plane loading for the different fiber angles. As the θ increase from 5 to 30, the critical loads increase and the maximum in-plane deflections decrease. By contrast, as the θ increase from 45 to 75, the load-deflection curves are significantly different. It may be noted that the load-deflection curves are influenced due to both shape and fiber angles of laminated composite plates.

Table 3 Displacements of damaged and undamaged four-layer laminated composite plates (θ/-θ/θ/-θ):$\bar{w}=w\times10^6$.

Crack ratio (T)	Angle (θ) Solutions		5	15	30	45
Undamaged	FEM (Present)	4×4	2.3640	2.2405	1.9973	1.8833
	Navier		2.3736	2.2541	2.0082	1.8955
0.1	FEM (Present)	4×4	2.4356	2.3200	2.0671	1.9464
	Navier		2.4546	2.3304	2.0738	1.9565
0.2	FEM (Present)	4×4	2.6489	2.5114	2.2236	2.0991
	Navier		2.6588	2.5222	2.2351	2.1044
0.3	FEM (Present)	4×4	2.9029	2.7426	2.4113	2.2655
	Navier		2.9147	2.7615	2.4270	2.2750
0.5	FEM (Present)	4×4	3.3829	3.2102	2.7466	2.5404
	Navier		3.4000	3.2166	2.7567	2.5502

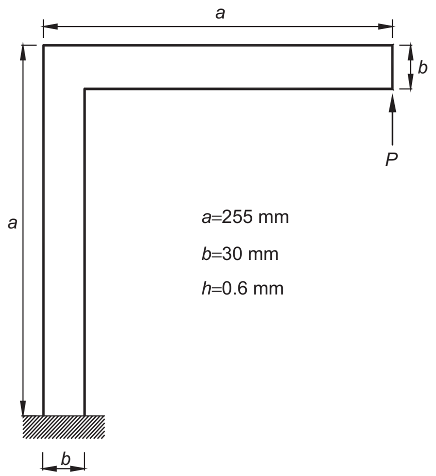

Figure 4 Clamped L-shaped plate subjected to in-plane load at the free end.

The load-deflection curve of L-shape laminated composite plate with the fiber angle of (23°/-23°/23°/-23°) laminate is higher than others. The difference does not exist almost when it is compared with the fiber angle of (30°/-30°/30°/-30°) laminate and does not express in Figure 7.

6.3. Laminated composite strip

The anti-symmetric (0°/90°) laminated composite plate (Figure 8) is considered. The two ends of the plate in the longitudinal direction are pinned at the supports and other edges are free.

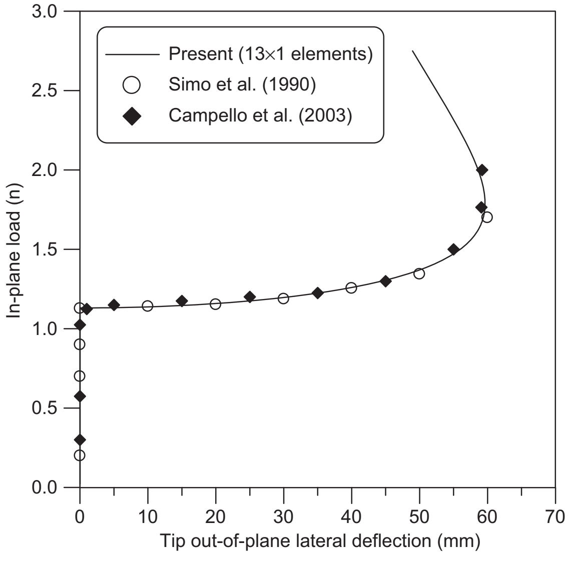

Figure 5 Out-of-plane deflection at the free end of the L-shaped plate.

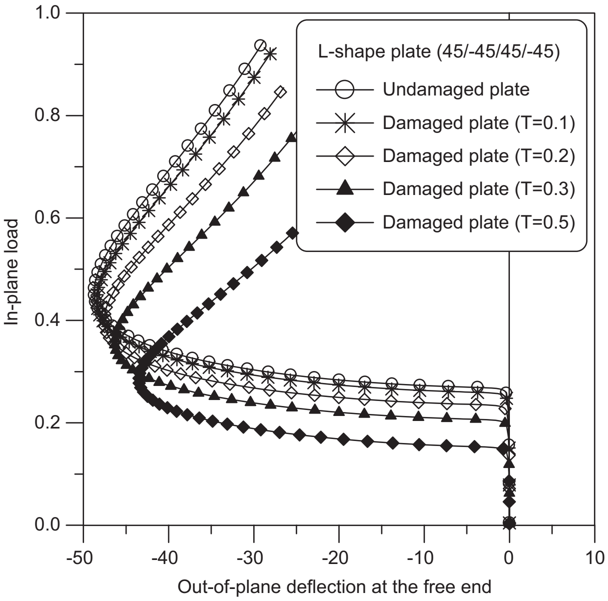

Figure 6 Tip deflection at the free end of the L-shaped laminated composite plate.

Reddy [15, 22] and Başar et al. [23] analyzed this problem using the higher-order and third-order shear deformation theory, respectively. The geometric and material properties are: the plate length, a=9.0 m, the plate width, b=1.5 m with thickness h=0.04 m, E_1=2.0×10^7 N/m^2, E_2=1.4×10^6 N/m^2, G_{12}=G_{13}=G_{23}=0.7×10^6 N/m^2, ν_{12}=0.3. Because of symmetry, a quarter of the plate was used in the model with nine shell elements. The results are shown in Figure 8 as displacement versus load factor plot.

It is noted that the results of the present theory are in very good agreement with those of Başar et al. [23] and Kreja and Schmidt [24]. It can be concluded from Figure 9 that the Reddy's higher-order transverse shear strains do not improve the accuracy of the results in thin-walled structures. Reddy's results [15, 22] are acceptable only for the range $w/h \leq 10$ due to his theory being based on the von Kármán plate theory [24]. Proven above, the results of the presented theory are in very good agreement with those of Başar et al. [23] and Kreja and Schmidt [24]. For a non-linear analysis it becomes important to select the Green strain tensor to obtain the higher performance of the laminated composite plates.

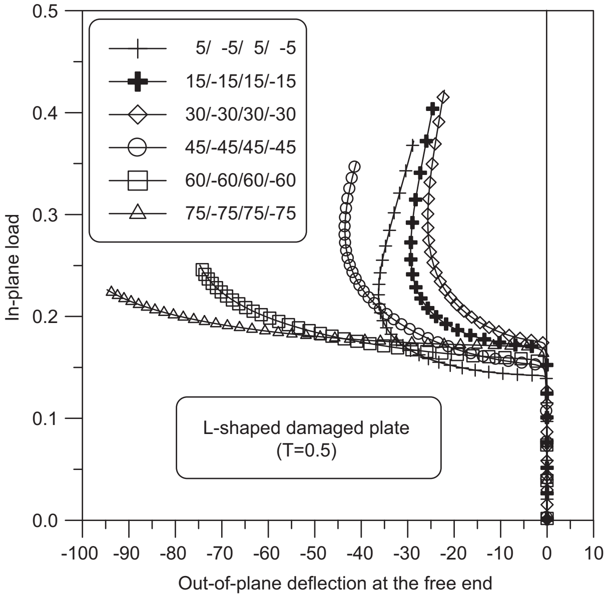

Figure 7 Tip deflection at the free end of the L-shaped damaged plate.

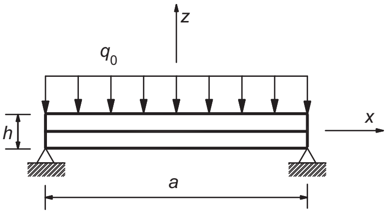

Figure 8 Geometry of laminated composite plate subjected to the distributed load.

The center deflections of undamaged and damaged composite plate strips under the increased loads are shown in Figure 10. The material properties of Table 2, V^f=0.45 and ξ=4.12 are used. For a plate with two numbers of layers (0°/90°), the center deflection of the damaged plate is significantly higher than that of the undamaged plate.

6.4. Laminated composite clamped shell

The non-linear problem of the clamped laminated composite shell is analyzed using a total thickness of 3.175 mm. As presented in Figure 11, the total length is L=508 mm, the radius of the circular edges is R=2540 mm and β=0.2 radians. If not declared otherwise, the material properties of Table 2, V^f=0.45 and ξ=4.12 are used in this study. Only a quarter of

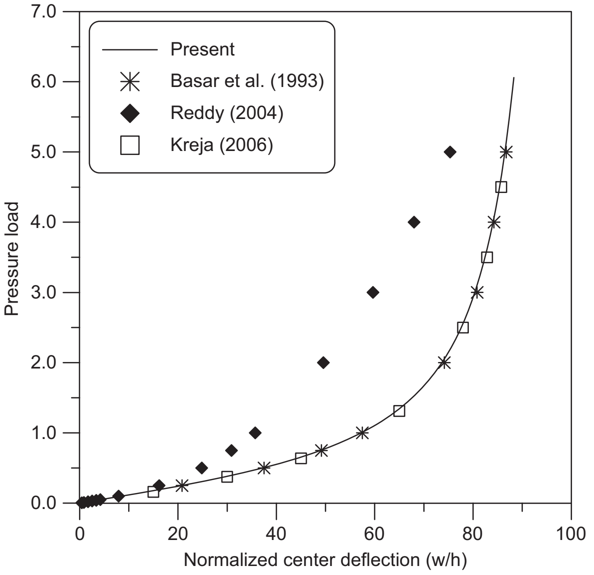

Figure 9 Load-deflection curve of laminated composite plate under pressure load.

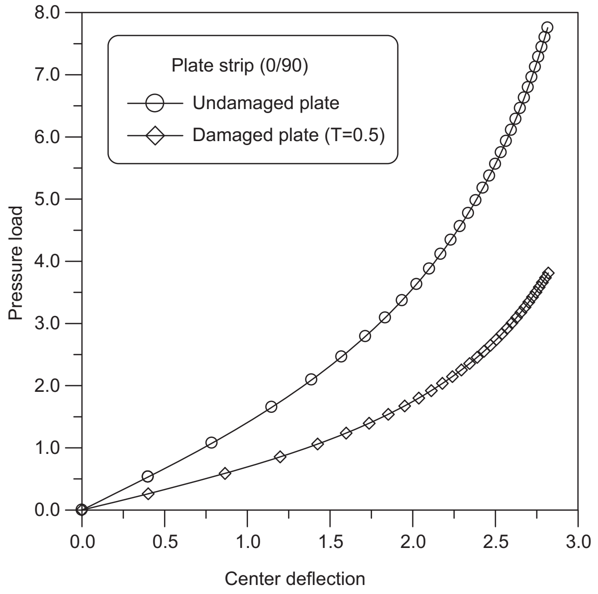

Figure 10 Load-deflection curve of laminated composite plate under pressure load.

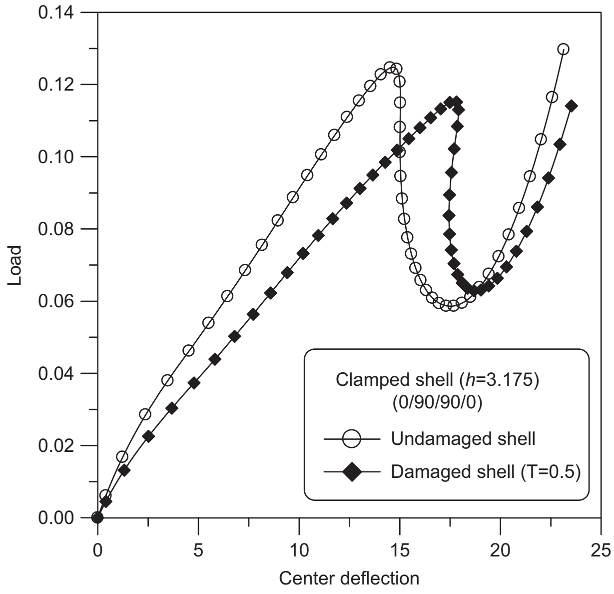

Figure 12 Load-displacement curves of clamped cylindrical shell.

the problem is modeled with 3×3 meshes. The laminate is composed of four layers (0°/90°/90°/0°). Figure 12 is presented for load-displacement curves of undamaged and damaged clamped shells. The load-displacement curve shows snap-through behavior with a sharp initial bifurcation.

In Figure 13, different mesh sizes are used to verify the shell element for composite clamped shell. Based on the mesh convergence study, a 3×3 mesh size could be used for the following analyses.

For various damage variables of the shells, the load-displacement curves are plotted in Figure 14. From this figure it can be observed that lower critical buckling load is obtained at higher values of damage variable. For the orthotropic ply orientation, Figures 15 and 16 show the influence of the number of layers on the load-central deflection of damaged clamped shells under point load. For the anti-symmetric orthotropic case, the critical loads for the four and eight number of layers are close to each other. By contrast, the induced critical load for the two numbers of layers is extremely higher than others. Furthermore, for the symmetric case shown in Figure 16, the load-central deflection curves are significantly different for different layer-up sequences.

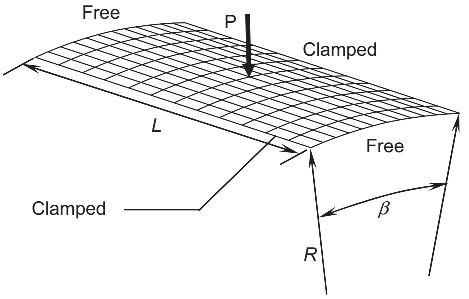

Figure 11 Geometry of clamped shell.

This observation provides us with a clue that it could be better to use a symmetric case in designing a lay-up sequence especially when the lateral point load is applied. In this case, a small number of layers results in better rigidity against applied loading.

6.5. Laminated composite hinged shell

A cylindrical hinged shell as shown in Figure 17 subjected to a concentrated load at the center point was analyzed. The total thickness of the laminated is h=6.35 mm and all layers have the same thickness.

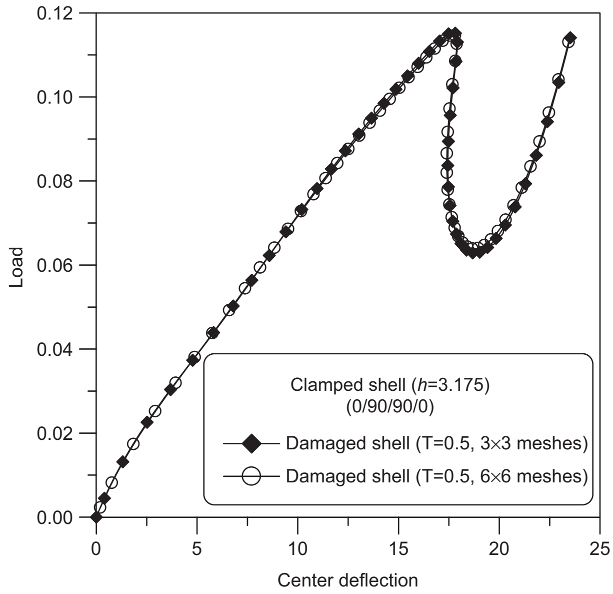

Figure 13 Load-displacement curves of clamped cylindrical shell.

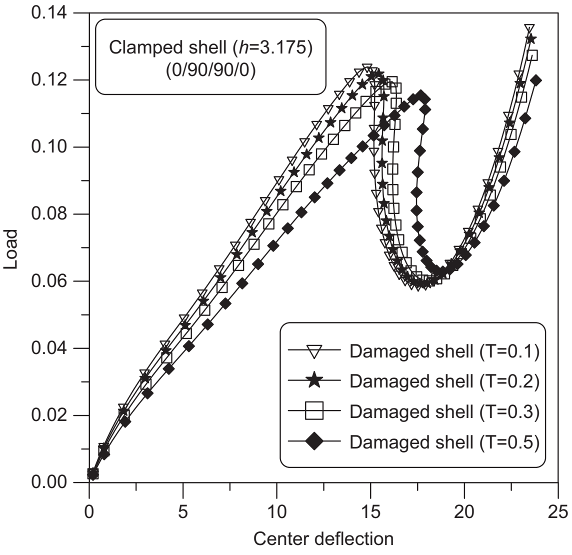

Figure 14 Load-displacement curves of clamped cylindrical shell.

The four layers cross-ply (0°/90°/90°/0°) and angle-ply (45°/-45°/45°/-45°) are considered in Figures 18 and 19. As expected, the load-deflection curve of undamaged hinged shells with the fiber angle of (0°/90°/90°/0°) and (45°/-45°/45°/-45°) exhibits the higher value than damaged hinged shells.

Load-displacement curves of composite shell with damage variable under point load is shown in Figure 20. The critical buckling load decreases slightly with the increase in damage variable.

Figures 21 and 22 show the load-deflection curves of orthotropic and angle-ply laminates. Even for the same fiber orientation, the difference becomes more dramatic for the case of different number of layers (four, six and eight layers). For the orthotropic case, the critical loads for the four and eight

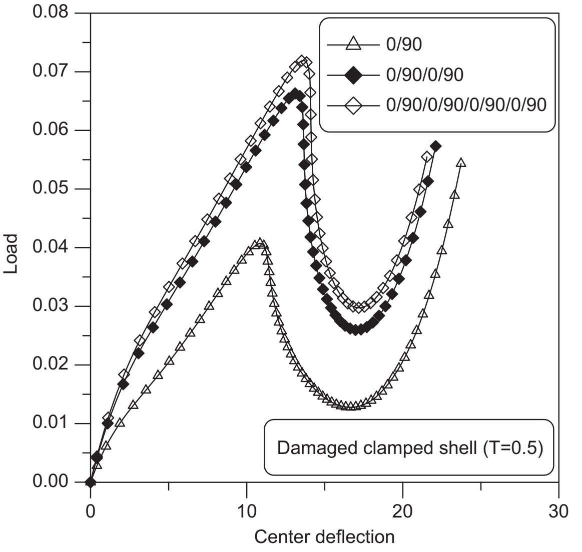

Figure 15 Load-displacement curves of clamped cylindrical shell.

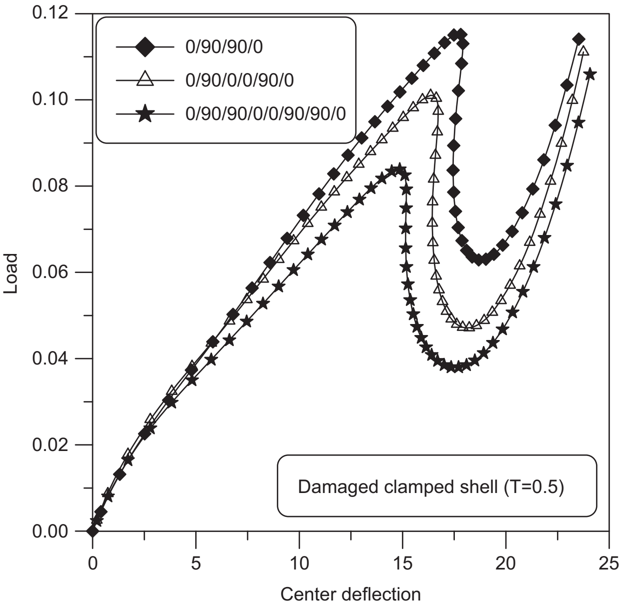

Figure 16 Load-displacement curves of clamped cylindrical shell.

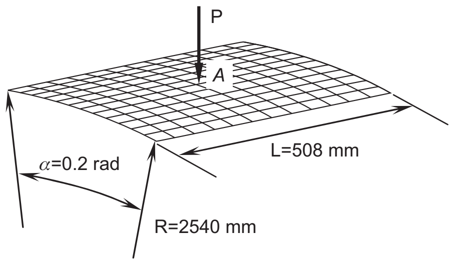

Figure 17 Geometry of cylindrical hinged shell.

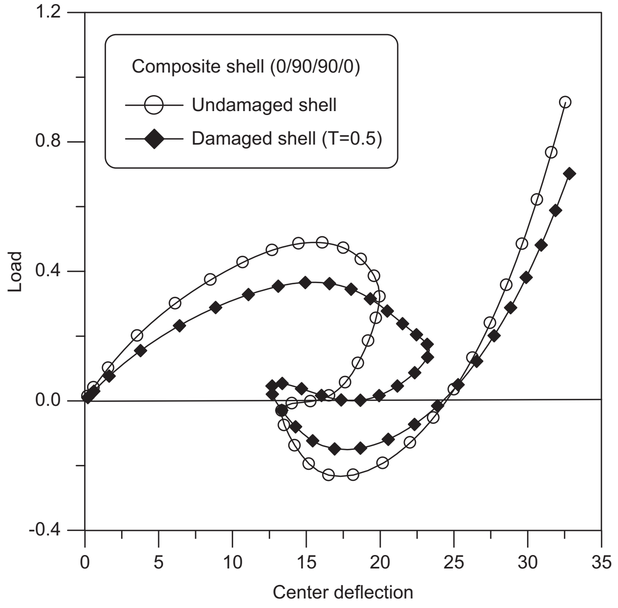

Figure 18 Load-displacement curves of hinged cylindrical shell.

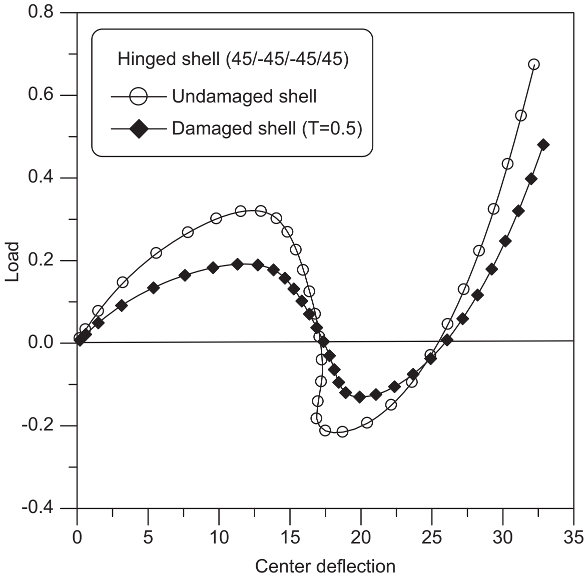

Figure 19 Load-displacement curves of hinged cylindrical shell.

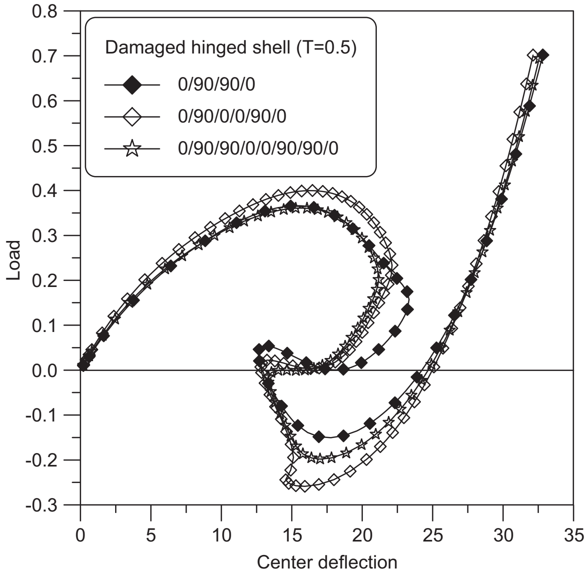

Figure 21 Load-displacement curves of hinged cylindrical shell.

number of layers are close to each other. By contrast, the critical load for the six numbers of layers is higher than others.

In Figure 22, for the angle-ply case, the post-buckling paths show similar trends regardless of the increasing number of layers and the critical loads of the damaged hinged shells increase slightly.

7. Conclusions

An intuitive prediction of the geometrically non-linear behavior of laminated composite structures under the multi-directional stiffness degradation is difficult because of their complexity and the combined effect of anisotropy, non-linear geometry and the shape of the structures. A stiffness degradation model for laminated composite induced by matrix cracks was developed based on the fracture mechanics theory, where the stiffness degradation constants of laminates are considered as a function of the damage variable T. Geometrically non-linear analysis of laminated composite thin shells using an element-based Lagrangian formulation is proposed. The present composite shell element formulation is based on "modified" first-order transverse shear deformation theory, which results in parabolic through-thickness distribution of the transverse shear strains and stresses. It eliminates the need for shear correction factors

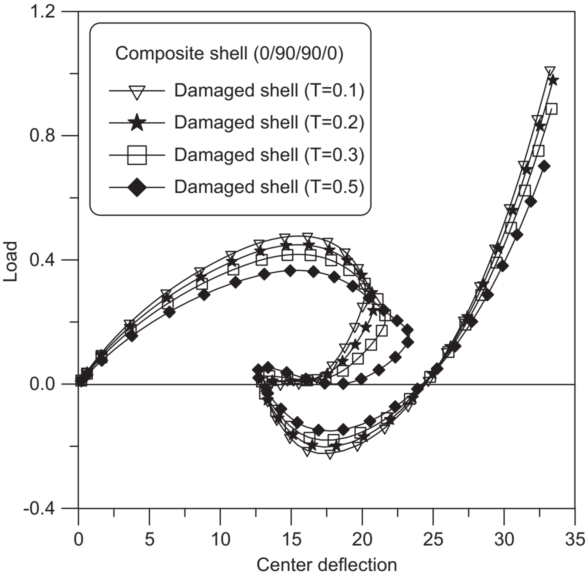

Figure 20 Load-displacement curves of hinged cylindrical shell.

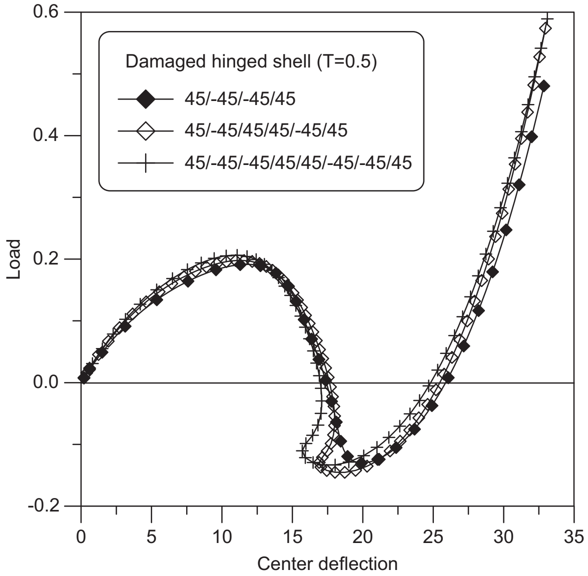

Figure 22 Load-displacement curves of hinged cylindrical shell.

in the first-order theory. To overcome the limit in the very thin plates and shells, shear and membrane locking is avoided by using assumed natural strains. The advanced finite element non-linear analysis shows the significance of crack ratios and structure geometry for damaged plates and shells. In the case of the damaged L-shape composite plate, it may be noted that the load-deflection curves are influenced due to both shape and fiber angles of composite plates. For damaged clamped shells, it might be better to use a symmetric case in designing a lay-up sequence especially when the lateral point load is applied. In this case, a small number of layers results in better rigidity against applied loading.

In general, the effect of damage variable T is to reduce the critical buckling load. The load-displacement curves of clamped shell shows snap-through behavior with a sharp initial bifurcation. The orthotropic case of hinged shell shows the snap-back behavior with a smooth initial bifurcation. The boundary conditions are demonstrated to be important for the behavior of composite laminates. Different boundary conditions can make a considerable difference in the resistance of the shell against collapse.

The results of this study may serve as a benchmark for future guidelines in designing laminated composite plates and shells under the multi-directional stiffness degradation. However, our parametric study is only an example and more studies should be carried out for individual cases.

References

[1] Talerja R. *Fatigue of Composite Materials*, Technomic Publishing Co., Inc.: Lancaster, PA, 1987.

[2] Yao WX, Himmel N. *Compos. Sci. Technol.* 2000, 60, 59–64.

[3] Byrd LW, Birman V. *Int. J. Mechan. Sci.* 2002, 44, 2173–2187.

[4] Lim SG, Hong CS. *J. Compos. Mater.* 1989, 23, 695–713.

[5] Talerja R. *Eng. Fract. Mechan.* 1986, 25, 751–762.

[6] Fujii T, Kawakami H, Morita Y. *J. Reinforc. Plast. Compos.* 1996, 15, 183–195.

[7] Duan X, Yao WX. *Int. J. Fatigue* 2002, 24, 119–125.

[8] Huang HC, Hinton E. *Int. J. Num. Meth. Eng.* 1986, 22, 73–92.

[9] MacNeal RH. *Nucl. Eng. Design* 1982, 33, 1049–1058.

[10] Dvorkin EN, Bathe KJ. *Eng. Computat.* 1984, 1, 77–88.

[11] Kanok-Nukulchai W, Wong WK. *Comput. Struct.* 1988, 30, 967–974.

[12] Tanov R, Tabiei A. *Finite Elem. Anal. Des.* 2000, 35, 189–197.

[13] Han SC, Ham HD, Kanok-Nukulchai W. *Int. J. Non-linear Mechan.* 2008, 43, 53–64.

[14] Tsai SW. *Composite Design*, 4th ed., Think Composites: Dayton, OH, 1988.

[15] Reddy JN. *Mechanics of Laminated Composite Plates and Shells*, CRC Press: Boca Raton, FL, 2004.

[16] Kanok-Nukulchai W. *Int. J. Num. Meth. Eng.* 1979, 14, 179–200.

[17] Han SC, Choi S, Park WT. *Sci. Eng. Compos. Mater.* 2007, 14, 271–297.

[18] Crisfield MA. *Comput. Struct.* 1981, 13, 55–62.

[19] Zienkiewicz OC, Taylor RL. *The Finite Element Method*, Butterworth-Heinemann: London, 2000.

[20] Campello EMB, Pimenta PM, Wriggers P. *Computat. Mechan.* 2003, 31, 505–518.

[21] Simo JC, Fox DD, Rifai MS. *Comput. Meth. Appl. Mechan. Eng.* 1990, 79, 21–70.

[22] Reddy JN. *Int. J. Non-linear Mechan.* 1990, 25, 677–686.

[23] Başar Y, Ding Y, Schultz R. *Int. J. Solids Struct.* 1993, 30, 2611–2638.

[24] Kreja I, Schmidt R. *Int. J. Non-linear Mechan.* 2006, 41, 101–123.